Skeletal Muscle–Specific Deletion of MKP-1 Reveals a p38 MAPK/JNK/Akt Signaling Node That Regulates Obesity-Induced Insulin Resistance

Ahmed Lawan,[1] Kisuk Min,[1] Lei Zhang,[1] Alberto Canfran-Duque,[2,3] Michael J. Jurczak,[4] Joao Paulo G. Camporez,[4] Yaohui Nie,[5] Timothy P. Gavin,[5] Gerald I. Shulman,[4] Carlos Fernandez-Hernando,[2,3] and Anton M. Bennett[1,2,3]

Diabetes 2018;67:624–635 | https://doi.org/10.2337/db17-0826

SIGNAL TRANSDUCTION

Stress responses promote obesity and insulin resistance, in part, by activating the stress-responsive mitogen-activated protein kinases (MAPKs), p38 MAPK, and c-Jun NH_2-terminal kinase (JNK). Stress also induces expression of MAPK phosphatase-1 (MKP-1), which inactivates both JNK and p38 MAPK. However, the equilibrium between JNK/p38 MAPK and MKP-1 signaling in the development of obesity and insulin resistance is unclear. Skeletal muscle is a major tissue involved in energy expenditure and glucose metabolism. In skeletal muscle, MKP-1 is upregulated in high-fat diet–fed mice and in skeletal muscle of obese humans. Mice lacking skeletal muscle expression of MKP-1 (MKP1-MKO) showed increased skeletal muscle p38 MAPK and JNK activities and were resistant to the development of diet-induced obesity. MKP1-MKO mice exhibited increased whole-body energy expenditure that was associated with elevated levels of myofiber-associated mitochondrial oxygen consumption. miR-21, a negative regulator of PTEN expression, was upregulated in skeletal muscle of MKP1-MKO mice, resulting in increased Akt activity consistent with enhanced insulin sensitivity. Our results demonstrate that skeletal muscle MKP-1 represents a critical signaling node through which inactivation of the p38 MAPK/JNK module promotes obesity and insulin resistance.

Skeletal muscle is considered to be a major tissue for the disposal of glucose and free fatty acids and as such plays a critical role in the regulation of whole-body glucose metabolism and energy homeostasis (1–4). Skeletal muscle consists of myofibers that are classified as slow-twitch/oxidative myofibers that express type I myosin heavy chain (MHC) and fast-twitch/glycolytic myofibers that express type IIa, IIx, and IIb MHCs (5). A reduction in the proportion of type I myofibers, which are mitochondria rich, is observed in obesity, and the proportion of type I myofibers positively correlates with overall metabolic health (2,5–9).

Stress-responsive mitogen-activated protein kinases (MAPKs), p38 MAPK, and the c-Jun NH_2-terminal kinase (JNK) are important regulators of skeletal muscle metabolic function (10–12). The stress-responsive MAPKs control processes such as insulin signaling, glucose homeostasis, fatty acid metabolism, and energy expenditure (11,13–16). Although it is realized that metabolic stressors such as inflammation and nutrient excess activate both p38 MAPK and JNK (12,17), the results of these studies reflect the individual actions of these MAPKs on metabolism. It remains unknown as to what the integrated actions are of skeletal muscle stress-responsive MAPKs, such as p38 MAPK and JNK, on the progression of obesity and insulin resistance.

[1]Department of Pharmacology, Yale University School of Medicine, New Haven, CT
[2]Department of Comparative Medicine, Yale University School of Medicine, New Haven, CT
[3]Program in Integrative Cell Signaling and Neurobiology of Metabolism, Yale University School of Medicine, New Haven, CT
[4]Cellular & Molecular Physiology and Department of Internal Medicine, Section of Endocrinology and Metabolism, Yale University School of Medicine, New Haven, CT
[5]Department of Health and Kinesiology, Purdue University, West Lafayette, IN

Corresponding author: Anton M. Bennett, anton.bennett@yale.edu.

Received 16 July 2017 and accepted 3 January 2018.

This article contains Supplementary Data online at http://diabetes.diabetesjournals.org/lookup/suppl/doi:10.2337/db17-0826/-/DC1.

M.J.J. is currently affiliated with the Department of Endocrinology, University of Pittsburgh School of Medicine, Pittsburgh, PA, and Centre for Metabolism and Mitochondrial Medicine, University of Pittsburgh School of Medicine, Pittsburgh, PA.

Inactivation of the stress-responsive MAPKs is achieved by the specific dephosphorylation of the MAPKs by dual-specificity MAPK phosphatases (MKPs) (18). The MKPs have been implicated in the regulation of metabolic homeostasis (19). MKP-1, which dephosphorylates JNK and p38 MAPK, is an important regulator of MAPK-dependent regulation of lipid homeostasis, energy metabolism, and mitochondrial biogenesis (20,21). In skeletal muscle of obese mice, MKP-1 is upregulated by free fatty acids concomitant with downregulation of p38 MAPK (22). Whole-body MKP-1–deficient mice are resistant to diet-induced obesity, exhibit increased peroxisome proliferator–activated receptor γ coactivator 1α (PGC-1α) activity in skeletal muscle, and are protected from the loss of oxidative myofibers (22). Although these observations suggest a role for MKP-1 in skeletal muscle metabolism, the limitations of whole-body MKP-1 deletion (20) preclude definitive assessment of the contribution of MKP-1 in skeletal muscle toward systemic energy homeostasis and glycemic control. Therefore, the goal of this study was to address the contribution of skeletal muscle MKP-1 toward glucose disposal and energy metabolism.

In this study, we found that in skeletal muscle, MKP-1 is overexpressed in obese humans. Our studies imply that when overexpressed, skeletal muscle MKP-1 contributes to obesity by antagonizing p38 MAPK and JNK, resulting in dysfunctional mitochondrial biogenesis and skewing of type I myofiber composition. These results demonstrate that it is the opposing action of skeletal muscle MKP-1 on the p38 MAPK/JNK module, which reflects a nodal point of interference that leads to metabolic imbalance and susceptibility to obesity.

RESEARCH DESIGN AND METHODS

Reagents, Antibodies, and Immunoblotting

All reagents were procured from standard chemical vendors. Phospho-p38 MAPK (#9215S), phospho-JNK1/2 (#4668S), phospho–extracellular signal–regulated kinase 1/2 (ERK1/2; #9101S), phospho-Akt (#9271S), phospho-p70 S6 kinase (#9234S), Akt1 (#2938S), p70 S6 kinase (2708S), PTEN (#9559S), and α-tubulin (#3873S) were obtained from Cell Signaling Technology (Danvers, MA). ERK1/2 (#sc-94), p38 MAPK (#sc-535), JNK (#sc-571), and MKP-1 (#sc-1199) were obtained from Santa Cruz Biotechnology (Santa Cruz, CA). Skeletal muscle tissue from chow- and high-fat diet (HFD)–fed male *Mkp-1*$^{fl/fl}$ and mice lacking skeletal muscle expression of MKP-1 (MKP-MKO) was isolated as described (23).

Animal and Human Studies

Generation of MKP-1 "floxed" mice has been described (23). MKP-1 flox/flox (*Mkp-1*$^{fl/fl}$) mice were bred with mice expressing Cre recombinase under the control of human α-skeletal actin (HSA-Cre) (24) to obtain HSA-Cre-MKP-1flox/+ that were backcrossed to *Mkp-1*$^{fl/fl}$ mice to generate skeletal muscle–specific deletion of MKP-1, HSA-Cre-MKP-1$^{fl/fl}$; referred to as MKP-1 skeletal muscle knockout mice (MKP1-MKO). Muscle biopsy samples from healthy, sedentary lean and obese individuals between the ages of 18 and 35 years were used. Lean individuals had a BMI <25 kg/m^2, and obese individuals had a BMI ≥ 30 kg/m^2.

Metabolic Measurements

Glucose tolerance tests (GTTs) were carried out in 8–12-week-old male *Mkp-1*$^{fl/fl}$ and MKP-MKO littermates. Mice were fasted overnight for 16 h followed by an i.p. injection of glucose (2 g/kg). Blood glucose was measured at 0, 15, 30, 60, 90, and 120 min. For insulin tolerance tests (ITTs), mice were fasted for 4 h and injected (i.p.) with 0.5 mU/g human insulin (Humulin R; Eli Lilly and Company, Indianapolis, IN). Hyperinsulinemic-euglycemic clamp studies were carried out on male chow-fed *Mkp-1*$^{fl/fl}$ and MKP1-MKO mice at 12 weeks old at the Yale Metabolic Phenotyping Center as described (23). Conscious male *Mkp-1*$^{fl/fl}$ and MKP1-MKO mice were used to determine total body fat and lean mass using ^{1}H-magnetic resonance spectroscopy (Bruker mini-spec Analyzer; Echo Medical Systems, Houston, TX). Mice were adapted for 2 weeks, kept in metabolic cages (TSE Systems, Bad Homburg, Germany) for 1 week, and food and water intake, energy expenditure, respiratory exchange ratio (RER), and physical activity were measured (23).

Cell Culture and Transient Transfections

C2C12 myoblasts were cultured as described (22) and transfected with constitutively active mutants of MKK6 (EE), MKK4 (EE), and MEK1 (23) in the absence or presence of 5 μmol/L MAPK inhibitors of SB203580 (p38 MAPK), SP600125 (JNK), and U0126 (MEK). After 48 h, myoblasts were lysed using RIPA buffer (23).

Skeletal Muscle Mitochondrial Oxygen Consumption and DNA Quantitation

For mitochondrial oxygen consumption, samples of muscle from chow- and HFD-fed male *Mkp-1*$^{fl/fl}$ and MKP1-MKO mice were analyzed in a respiration chamber (23). Total DNA was isolated from soleus muscle using QIAamp DNA mini kit (Qiagen, Hilden, Germany). Mitochondrial DNA (mtDNA) was quantified by quantitative RT-PCR using primers amplifying the D-loop region on mtDNA.

RNA Extraction and Real-time PCR Analysis

Real-time quantitative PCR was carried out in triplicate with the Applied Biosystems 7500 Fast RT-PCR system (Applied Biosystems, Foster City, CA) and TaqMan and SYBR Green gene expression master mix for the following genes: *MKP-1*, sterol regulatory element-binding protein 1c (*SREBP1C*), *PPARG*, *PPARGC1B*, *PRC*, *c-Myc*, *p53*, *Spot14*, and *ME*. The following TaqMan primers (Applied Biosystems) were used: *PGC-1α*, Mn01208835_m1; *NDUFS1*, Mn00523631_m1; *NRF1*, Mn00447996_m1; *GABPA*, Mn00484598_m1; *NDUFB5*, Mn00452592_m1; *MFN2*, Mn01255785; and *TFAM*, Mn00447485_m1. TaqMan primers and gene expression master mix from Applied Biosystems were used for miR-21 and *MKP-1* quantitation.

Treadmill Exercise Training

Animals in the exercise-trained groups were habituated to running on a treadmill (Columbus Instruments, Columbus, OH) by increasing the duration and speed of running for 5 consecutive days. After habituation, animals were rested for 2 days and then performed 5 consecutive days of treadmill running for 60 min/day at 15 m/min, 0% grade. After 5 days of training, we performed a progressive exercise stress test. Maximum exercise capacity was determined by graded increase in treadmill speed (2 m/min to 6 m/min every 5 min) to exhaustion and then VO_{2max} and running distance were measured.

Measurement of Blood Chemistries

Serum and hepatic triglycerides were measured at the Yale Mouse Metabolic Phenotyping Center. Male chow-fed *Mkp-1*$^{fl/fl}$ and MKP1-MKO mice between 8 and 12 weeks old were used for the measurement of plasma glucose concentrations by a glucose oxidase method using a Beckman Glucose Analyzer II (Beckman Coulter, Sharon Hill, PA). The measurement of plasma insulin was performed by radioimmunoassay (Linco Research, St. Louis, MO). Oil Red O staining was performed as described (23).

Statistical Analysis

All data represent the mean ± SEM. Differences between groups were calculated using a Student *t* test or ANOVA with Bonferroni posttest for multiple comparisons using Prism 6 statistical software (GraphPad Software, La Jolla, CA).

RESULTS

MKP-1 Overexpression in Skeletal Muscle of Obese Humans

Aberrant skeletal muscle expression of MKP-1 could play a role in the progression of obesity and insulin resistance in humans. We determined the expression levels of MKP-1 in skeletal muscle of lean and obese human subjects. In skeletal muscle of obese subjects, we found that the expression levels of MKP-1 protein were significantly elevated (~40%; $P < 0.05$; $N = 7$) as compared with lean subjects (Fig. 1*A*). Concomitantly, p38 MAPK was significantly downregulated in obese subjects (Fig. 1*A*). These results suggest that MKP-1 overexpression in skeletal muscle of humans may contribute to the development of obesity and/or insulin resistance.

MKP1-MKO Mice Are Resistant to Diet-Induced Obesity

To examine the role of MKP-1 in skeletal muscle, we bred MKP-1 "floxed" mice (23) with the HSA-Cre mice (24) to produce offspring in which MKP-1 is deleted specifically in skeletal muscle (MKP1-MKO) (Fig. 1*B*). MKP1-MKO mice displayed increased skeletal muscle p38 MAPK and JNK, but not ERK1/2, phosphorylation (Fig. 1*C*). Therefore, deletion of skeletal muscle MKP-1 results in the upregulation of both p38 MAPK and JNK phosphorylation, indicating functional loss of MKP-1.

Male MKP1-MKO mice fed a chow diet exhibited comparable weight gain and total body lean mass, but significantly reduced fat mass, as compared with *Mkp-1*$^{fl/fl}$ littermate controls (Fig. 1*D–F*). Skeletal muscle sections and weights showed no differences between chow-fed MKP1-MKO and *Mkp-1*$^{fl/fl}$ littermate controls (Fig. 1*G* and *H*). No differences either in weight or histological presentation were observed in the liver or adipose tissue of chow-fed MKP1-MKO mice (Supplementary Fig. 1). MKP1-MKO mice fed an HFD had a significantly ($P < 0.01$) reduced rate of weight gain as compared with their *Mkp-1*$^{fl/fl}$ littermates (Fig. 2*A*). By 16 weeks of high-fat feeding, MKP1-MKO mice weighed ~20% less ($P < 0.01$) as compared with their *Mkp-1*$^{fl/fl}$ littermate controls (Fig. 2*A*). This was due to reduced adiposity rather than lean mass (Fig. 2*B* and *C*). Skeletal muscles from HFD-fed MKP1-MKO mice were unremarkable (Fig. 2*D*). Resistance to diet-induced obesity in MKP1-MKO mice was associated with reduced serum triglyceride accumulation (Fig. 2*E*) that occurred independently of changes in skeletal muscle lipogenic gene expression of *PPARG* and *SREBP1C* (Fig. 2*F* and *G*). These results demonstrate that loss of MKP-1 in skeletal muscle protects from diet-induced obesity.

Chow-fed male MKP1-MKO mice (8–12 weeks) exhibit significantly enhanced energy expenditure levels, oxygen consumption, and carbon dioxide output as compared with *Mkp-1*$^{fl/fl}$ littermate controls (Fig. 3*A–C*). No differences in RER, food intake, or activity between the two genotypes were observed (Fig. 3*D–F*). These results demonstrate that loss of MKP-1 in skeletal muscle is protective from diet-induced obesity because of increased energy expenditure.

Resistance to Hepatic Steatosis and Increased Insulin Sensitivity in MKP1-MKO Mice

Upon HFD feeding for 18 weeks, the livers of male MKP1-MKO mice were resistant to the acquisition of hepatic steatosis (Fig. 4*A*), as evidenced by a marked decrease in liver weight and hepatic triglyceride accumulation (Fig. 4*B* and *C*). Consistent with this, MKP1-MKO livers exhibited significantly decreased expression levels of *PPARG* and *SREBP1C* mRNA (Fig. 4*D* and *E*). MKP1-MKO and *Mkp-1*$^{fl/fl}$ controls displayed comparable levels of p38 MAPK, JNK (Fig. 4*F*), and Akt activities (Fig. 4*G*). Together, these results show that skeletal muscle MKP1-MKO mice, when fed an HFD, exhibit impaired hepatic de novo lipogenesis independently of p38 MAPK, JNK, Erk, and Akt activities.

Under conditions of chow and HFD feeding, MKP1-MKO mice and *Mkp-1*$^{fl/fl}$ controls were comparable in their basal glucose levels (Fig. 5*A*). However, MKP1-MKO mice exhibited significantly reduced plasma insulin levels as compared with *Mkp-1*$^{fl/fl}$ controls under both fasted and fed conditions (Fig. 5*B*). These results suggested that MKP1-MKO mice were more insulin sensitive than *Mkp-1*$^{fl/fl}$ controls and required less insulin to maintain euglycemia. On a chow diet, GTTs and ITTs in MKP1-MKO mice were comparable (Fig. 5*C* and *D*), and this was confirmed by hyperinsulinemic-euglycemic clamp analyses (Supplementary Fig. 2). GTTs showed that MKP1-MKO mice managed an acute glucose load to levels that were comparable to

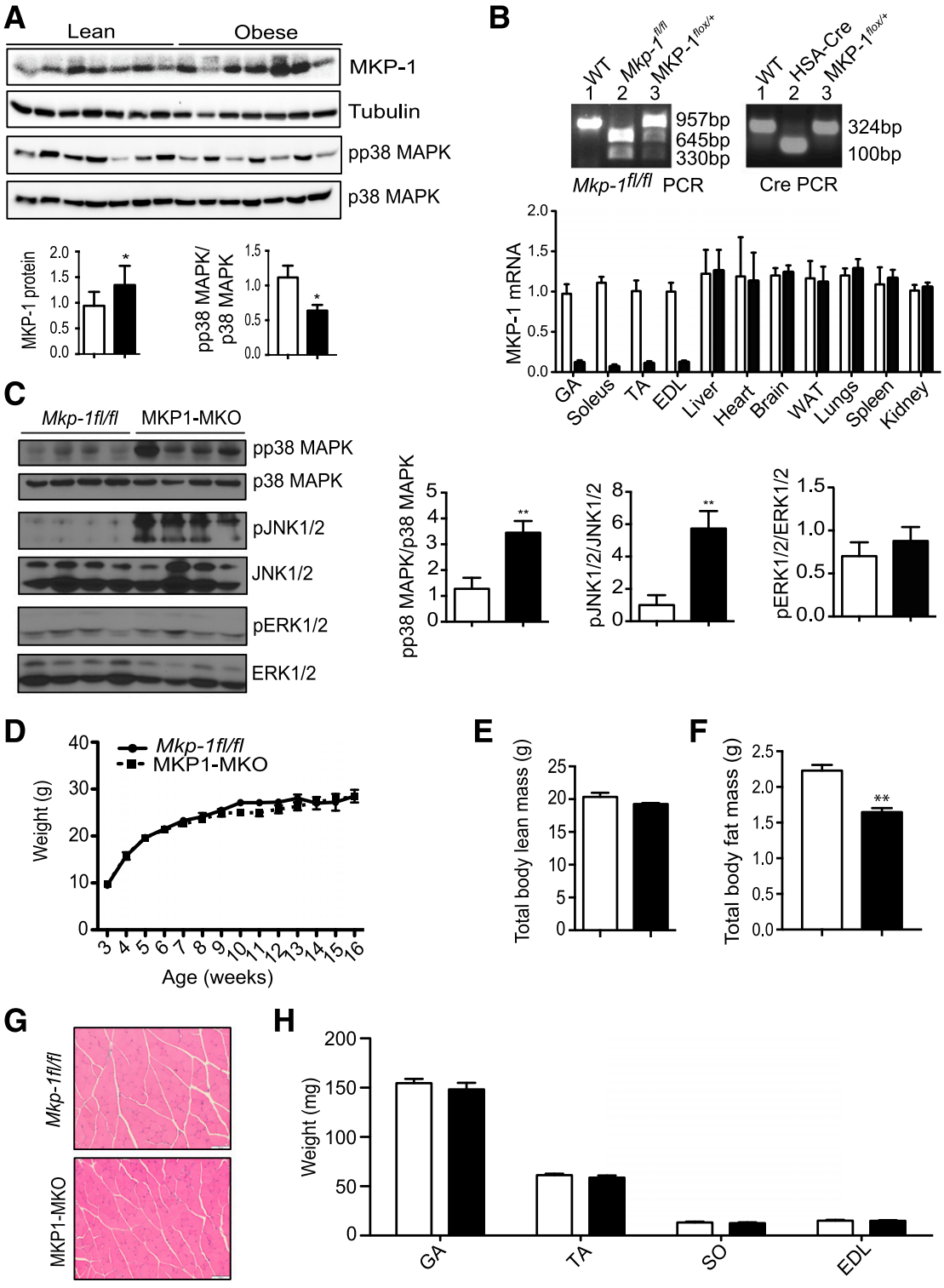

Figure 1—Generation and characterization of mice with skeletal muscle–specific deletion of MKP-1. *A*: MKP-1 protein expression and phospho-(p)p38 MAPK/p38 MAPK from skeletal muscles of lean (BMI <25 kg/m^2) and obese (BMI <30 kg/m^2) human subjects (n = 7). *B*: *Mkp-1*$^{fl/fl}$ and MKP1-MKO genotyping (top panel) and MKP-1 mRNA expression from various tissues in chow-fed *Mkp-1*$^{fl/fl}$ and MKP1-MKO mice (bottom panel) (n = 8–10). *C*: Immunoblots of skeletal muscle lysates from chow-fed *Mkp-1*$^{fl/fl}$ and MKP1-MKO mice for pp38 MAPK, pJNK1/2, and pERK1/2 normalized to corresponding total MAPKs (left panel). Immunoblots were quantitated by densitometry (right panels). Weight curves (*D*), total body lean mass (*E*), and total body fat mass (*F*). Hematoxylin and eosin staining of skeletal muscle sections (*G*) and skeletal muscle weights (*H*) of chow-fed male *Mkp-1*$^{fl/fl}$ and MKP1-MKO mice. Scale bars: 100 μm. Results represent n = 8/genotype, and data shown are the mean ± SEM. *$P < 0.05$; **$P < 0.01$ as determined by Student t test. White bars, *Mkp-1*$^{fl/fl}$ mice; black bars, MKP1-MKO mice. EDL, extensor digitorum longus; GA, gastrocnemius; SO, soleus; TA, tibialis anterior; WAT, white adipose tissue; WT, wild-type.

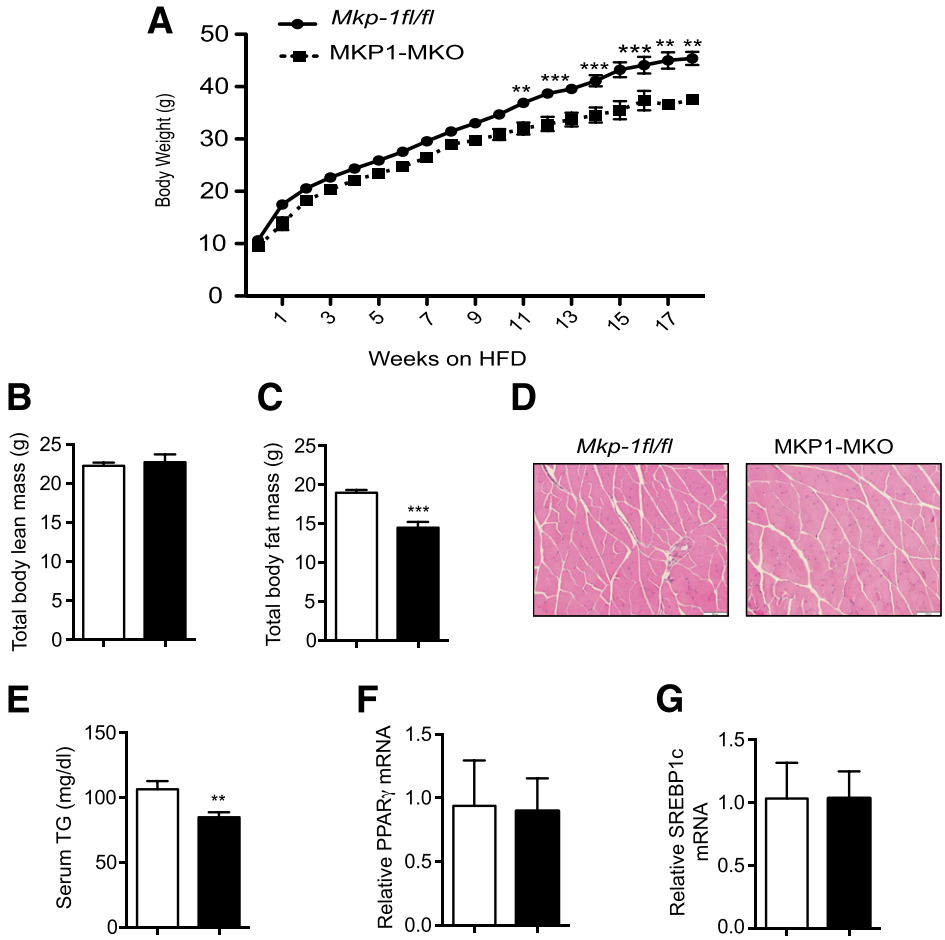

Figure 2—Resistance to diet-induced obesity in MKP1-MKO mice. *A*: Weight curves of HFD-fed male *Mkp-1*$^{fl/fl}$ and MKP1-MKO mice for 18 weeks. Spectroscopic analysis of total body lean mass (*B*) and fat mass (*C*) from HFD-fed *Mkp-1*$^{fl/fl}$ and MKP1-MKO mice (n = 9 to 10/genotype). *D*: Representative hematoxylin and eosin staining of skeletal muscle sections from HFD-fed *Mkp-1*$^{fl/fl}$ and MKP1-MKO mice. Scale bars: 100 μm. *E*: Serum triglycerides (TG) from HFD-fed *Mkp-1*$^{fl/fl}$ and MKP1-MKO mice (n = 6/genotype). Skeletal muscle mRNA expression of *PPARG* (*F*) and *SREBP1C* (*G*) from HFD-fed *Mkp-1*$^{fl/fl}$ and MKP1-MKO mice (n = 6/genotype). Data represent mean ± SEM. $^{**}P < 0.01$; $^{***}P < 0.0001$ as determined by Student t test or in ANOVA with Bonferroni posttest for multiple comparisons (*A*). White bars, *Mkp-1*$^{fl/fl}$ mice; black bars, MKP1-MKO mice.

Mkp-1$^{fl/fl}$ controls under HFD feeding conditions (Fig. 5*E*). However, during the GTT, MKP1-MKO mice produced lower levels of circulating insulin as compared with *Mkp-1*$^{fl/fl}$ controls (Fig. 5*F*). Furthermore, ITTs demonstrated that HFD-fed MKP1-MKO mice were insulin sensitive (Fig. 5*G*). Collectively, these data demonstrate that MKP1-MKO mice are protected from the development of insulin resistance when fed an HFD.

Enhanced Skeletal Muscle p38 MAPK, JNK, and Akt Signaling in MKP1-MKO Mice

To investigate the molecular basis for the enhanced insulin sensitivity in HFD-fed MKP1-MKO mice (Fig. 5), we measured the phosphorylation status of p38 MAPK, JNK, and ERK in skeletal muscles of HFD-fed MKP1-MKO mice. MKP1-MKO mice displayed increased levels of skeletal muscle p38 MAPK and JNK, but not ERK1/2, phosphorylation as compared with *Mkp-1*$^{fl/fl}$ controls (Fig. 6*A*). Remarkably, in skeletal muscles of MKP1-MKO mice, Akt Ser^{473} phosphorylation was significantly increased as compared with *Mkp-1*$^{fl/fl}$ controls (Fig. 6*B*). The phosphorylation of S6 kinase (S6K) Thr^{389} was also increased compared with that of *Mkp-1*$^{fl/fl}$ littermates (Fig. 6*B*). However, no significant differences in either Akt or S6K phosphorylation were observed between chow-fed MKP1-MKO and *Mkp-1*$^{fl/fl}$ littermate controls (Supplementary Fig. 3). These data demonstrate that MKP-1 in skeletal muscle plays a role in negatively regulating both p38 MAPK and JNK but additionally the Akt/S6K pathway in HFD-fed mice.

Skeletal Muscle MKP-1 Mediates Akt/PTEN Signaling Through miR-21

The observation that skeletal muscle MKP-1 negatively regulates Akt prompted us to examine the mechanism of MKP-1/Akt signaling cross talk. We first tested the idea that Akt signaling could be indirectly affected by alterations in the expression levels of PTEN, which negatively regulates Akt. When we assessed the expression levels of PTEN in

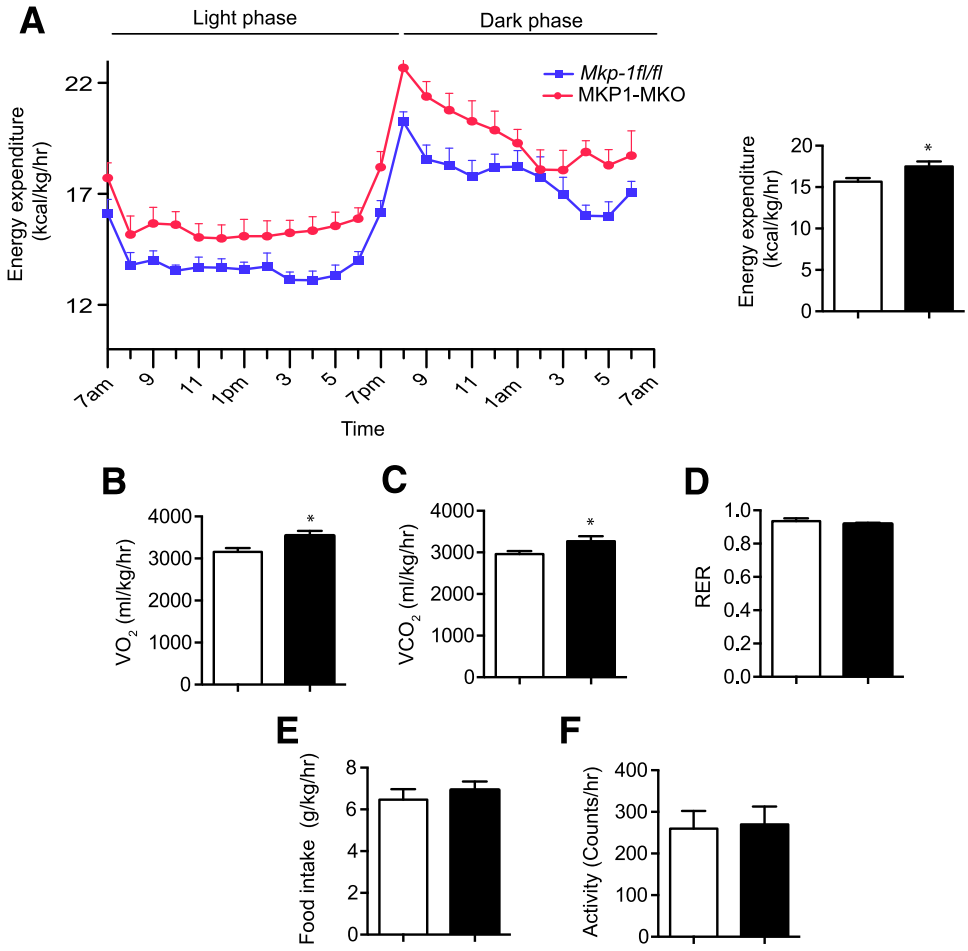

Figure 3—Increased whole-body energy expenditure in MKP1-MKO mice. *A–F*: Chow-fed *Mkp-1*$^{fl/fl}$ and MKP1-MKO mice were subjected to open circuit calorimetry. Energy expenditure (*A*), oxygen consumption (*B*), carbon dioxide production (*C*), RER (*D*), feeding (*E*), and locomotor activity (*F*) (n = 8/genotype). Data represent mean ± SEM. *$P < 0.05$ as determined by Student t test. White bars, *Mkp-1*$^{fl/fl}$ mice; black bars, MKP1-MKO mice.

skeletal muscles of HFD-fed MKP1-MKO mice, we found significantly reduced levels as compared with *Mkp-1*$^{fl/fl}$ controls (Fig. 7*A*). Consistent with the observation that the expression levels of Akt Ser^{473} were unaltered in the liver of MKP1-MKO mice, PTEN expression was unchanged between MKP1-MKO and *Mkp-1*$^{fl/fl}$ controls (Supplementary Fig. 4). These data suggest that in skeletal muscle, MKP-1 negatively regulates Akt activity by controlling PTEN expression.

It has been reported that one of the miR-21 targets is PTEN mRNA, which causes a decrease in the expression of PTEN (25,26). The expression levels of miR-21 were significantly increased in skeletal muscle of MKP1-MKO mice as compared with *Mkp-1*$^{fl/fl}$ littermates but not in the liver (Fig. 7*B*), where Akt phosphorylation is unaffected (Fig. 4*G*). The synthesis of mature microRNA (miRNA) starts with the formation of primary (pri-)miRNAs in the nucleus (27). Pri-miRNAs are further cleaved into precursor miRNAs in the cytoplasm into mature miRNAs (27). Therefore, we measured pri-miR-21 in skeletal muscles of MKP1-MKO mice. In addition to the enhanced levels of mature skeletal muscle miR-21 (Fig. 7*B*), MKP1-MKO mice exhibited increased expression of pri-miR-21 as compared with *Mkp-1*$^{fl/fl}$ littermates (Fig. 7*B*). However, pri-miR-21 levels were unaltered in its level of expression in the liver between genotypes (Fig. 7*B*). To substantiate the results of the pri-miR-21/miR-21 expression in the liver, we measured hepatic PTEN expression in MKP1-MKO mice. As expected, the expression of hepatic PTEN is equivalent between MKP1-MKO mice and *Mkp-1*$^{fl/fl}$ controls (Supplementary Fig. 4). These results support the notion that MKP-1 negatively regulates the miR-21/PTEN/Akt pathway in skeletal muscle.

To determine the MAPK dependency for the increase in miR-21 expression, C2C12 myoblasts were transfected with activating mutants of MKK6, MKK4, and MEK1 in order to constitutively activate p38 MAPK, JNK, and ERK, respectively (Fig. 7*C* and Supplementary Fig. 5*A*). Both activating mutants of MKK6 and MKK4 enhanced miR-21 expression (Fig. 7*C*). In contrast, we did not observe any significance change in miR-21 expression with an MEK1-activating mutant (Fig. 7*C*). Next, C2C12 myoblasts were transiently transfected with activating mutants of MKK6, MKK4, and MEK1 in the absence or presence of MAPK inhibitors of

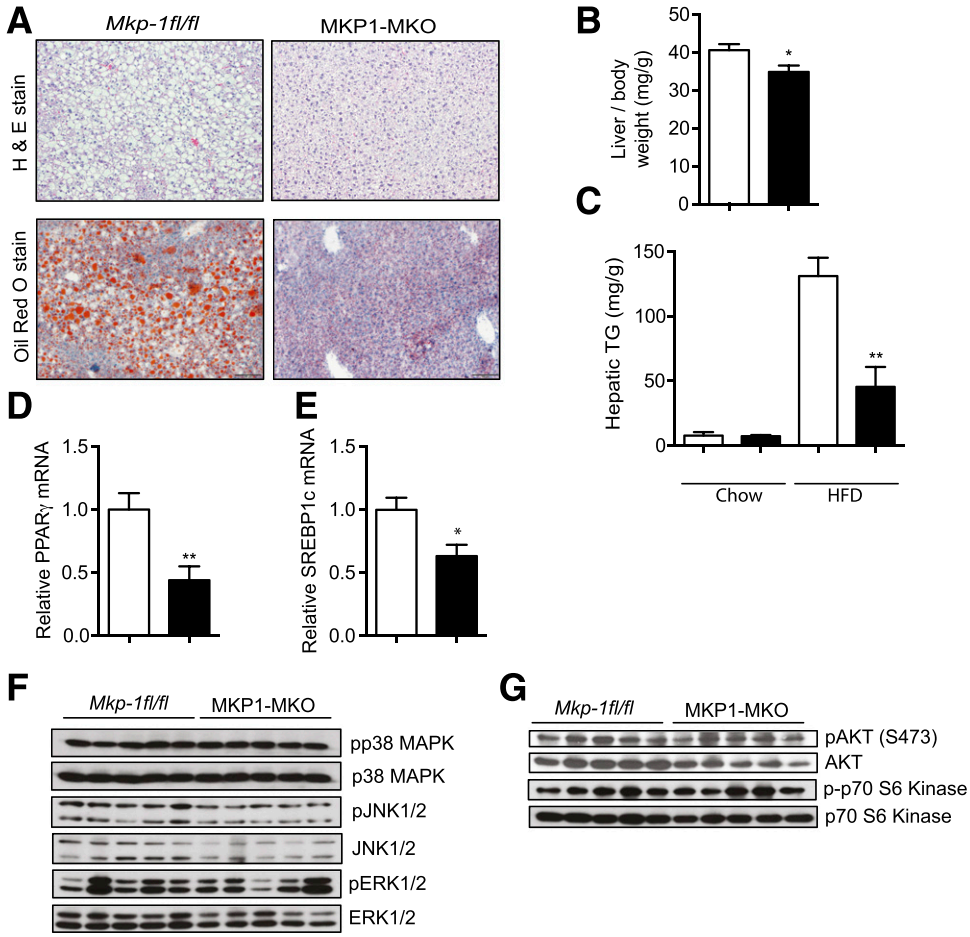

Figure 4—Protection from hepatosteatosis in MKP1-MKO mice. *A*: Representative hematoxylin and eosin (H & E) and Oil Red O staining of liver sections from HFD-fed *Mkp-1*$^{fl/fl}$ and MKP1-MKO mice. Scale bars: 100 μm. *B*: Liver to body weight ratio of HFD-fed *Mkp-1*$^{fl/fl}$ and MKP1-MKO mice (n = 9 to 10/genotype). *C*: Hepatic triglycerides (TG) from chow- and HFD-fed *Mkp-1*$^{fl/fl}$ and MKP1-MKO mice (n = 5 to 6/genotype). Hepatic mRNA expression of *PPARG* (*D*) and *SREBP1C* (*E*) from HFD-fed *Mkp-1*$^{fl/fl}$ and MKP1-MKO mice (n = 6/genotype). Liver lysates from HFD-fed *Mkp-1*$^{fl/fl}$ and MKP1-MKO mice were analyzed by immunoblotting for phospho-(p)p38 MAPK, pJNK1/2, and pERK1/2 shown with corresponding total MAPK (*F*) and pAkt and p-p70 S6K shown with corresponding Akt and p70 S6K totals (*G*). Results represent n = 5/genotype. Data represent mean ± SEM. *$P < 0.05$; **$P < 0.01$, as determined by Student t test. White bars, *Mkp-1*$^{fl/fl}$ mice; black bars, MKP1-MKO mice.

SB203580 (p38 MAPK), SP600125 (JNK), and U0126 (MEK) and miR-21 expression assessed. Both activating mutants of MKK6 and MKK4 enhanced miR-21 expression, which was inhibited in the presence of SB203580 and SP600125, respectively (Supplementary Fig. 5*B*). Whereas pharmacological inhibition of MEK1 in the presence of an activated MEK1 had no effect on miR-21 expression (Supplementary Fig. 5*B*). These data establish that MKP-1 negatively regulates Akt signaling by opposing p38 MAPK and/or JNK-mediated expression of miR-21 in skeletal muscle.

Skeletal Muscle MKP-1 Regulation of Myofiber Type Composition

Clinical studies from human skeletal muscles have demonstrated that obesity and insulin resistance are linked to a shift toward glycolytic myofibers concomitant with a reduction in oxidative myofiber fiber content (2,5–9). To evaluate the composition of myofiber types in MKP1-MKO mice, we measured the expression levels of MHC isoforms. In soleus muscle under both chow and HFD feeding conditions, the percentage of *MHCI* expression was significantly increased, whereas *MHCIIB* expression was reduced in MKP1-MKO mice as compared with *Mkp-1*$^{fl/fl}$ controls (Fig. 8*A*). The expression of *MHCIIA* and *MHCIIX* was comparable between the two genotypes (Fig. 8*A*). Similarly, tibialis anterior muscle revealed that *MHCI* expression was significantly increased concomitant with decreased levels of *MHCIIB* in MKP1-MKO mice compared with *Mkp-1*$^{fl/fl}$ controls fed chow and HFD (Fig. 8*B*). No differences were observed in the tibialis anterior of *MHCIIA* and *MHCIIX* between the genotypes (Fig. 8*B*). Collectively, these data demonstrated increased oxidative capacity in skeletal muscle of MKP1-MKO mice.

Enhanced Skeletal Muscle Mitochondrial Function in MKP1-MKO Mice

Next, we asked whether skeletal muscle mitochondrial genes were affected in MKP1-MKO mice. Under both chow and high-fat feeding, skeletal muscle PGC-1α, a master

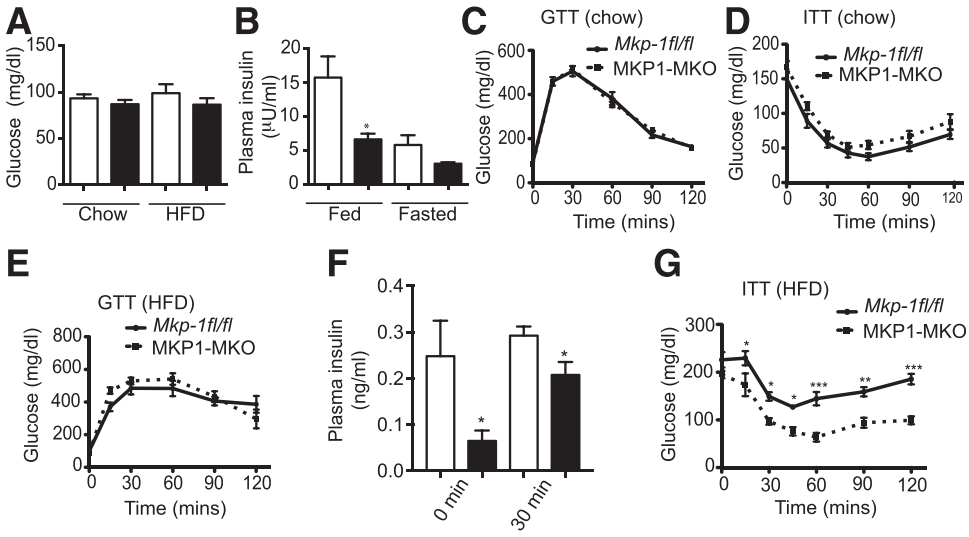

Figure 5—Insulin sensitivity in HFD-fed MKP1-MKO mice. Basal plasma glucose concentration in chow- and HFD-fed *Mkp-1*$^{fl/fl}$ and MKP1-MKO mice (*A*) and plasma insulin concentration in fed and overnight-fasted chow-fed *Mkp-1*$^{fl/fl}$ and MKP1-MKO mice (n = 8–10/genotype) (*B*). Plasma glucose concentration during GTTs (*C*) and ITTs (*D*) in overnight-fasted chow *Mkp-1*$^{fl/fl}$ and MKP1-MKO mice. GTT (*E*) and plasma insulin during GTT (*F*) and ITT (*G*) analyses in HFD-fed *Mkp-1*$^{fl/fl}$ and MKP1-MKO mice. Data represent n = 8–10/genotype. Mean ± SEM. $^{*}P < 0.05$; $^{**}P < 0.01$; $^{***}P < 0.0001$ as determined by Student t test and in *C–F* by ANOVA with Bonferroni posttest for multiple comparisons. White bars, *Mkp-1*$^{fl/fl}$ mice; black bars, MKP1-MKO mice.

regulator of mitochondrial biogenesis (28), was enhanced in expression in MKP1-MKO mice (Fig. 8*C* and *D*). A significant upregulation in the expression of *PGC-1β*, *TFAM*, *GABPα* and *NDUFS1* genes was detected in skeletal muscle of either chow- or HFD-fed MKP1-MKO mice (Fig. 8*C* and *D*). The expression of thyroid hormone target genes (29) *SPOT14* and *ME1* (malic enzyme) were also significantly increased in expression from skeletal muscle of chow-fed MKP1-MKO mice (Fig. 8*C*). The expression of *MYC*, which positively regulates mitochondrial biogenesis (30,31), was

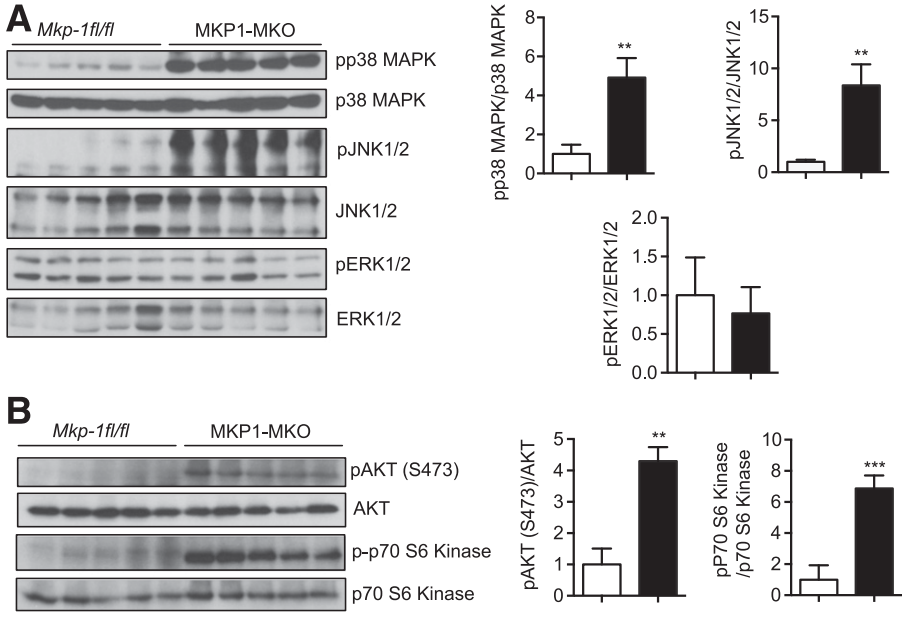

Figure 6—Enhanced MAPK and Akt signaling in skeletal muscle of HFD-fed MKP1-MKO mice. Skeletal muscle lysates from HFD-fed *Mkp-1*$^{fl/fl}$ and MKP1-MKO mice were analyzed by immunoblotting. Immunoblots were quantitated by densitometry for the levels of phospho-(p)p38 MAPK, pJNK1/2, and pERK1/2 normalized to corresponding total MAPKs (*A*) and pAkt and p-p70 S6K shown with corresponding Akt and p70 S6K totals (*B*). Results represent n = 5/genotype, and data shown are the mean ± SEM. $^{**}P < 0.01$; $^{***}P < 0.0001$ as determined by Student t test. White bars, *Mkp-1*$^{fl/fl}$ mice; black bars, MKP1-MKO mice.

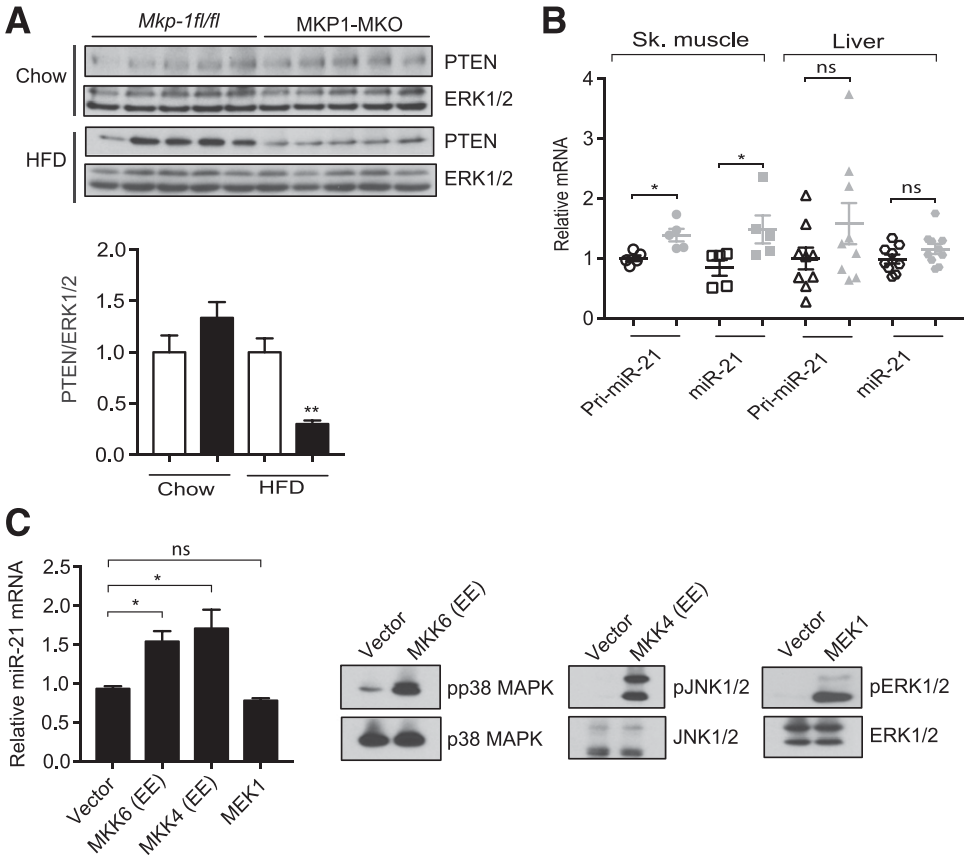

Figure 7—Skeletal muscle MKP-1 regulates Akt activity through PTEN/miR-21 in HFD-fed MKP1-MKO mice. *A*: Immunoblots from skeletal muscle of HFD-fed *Mkp-1*$^{fl/fl}$ and MKP1-MKO mice were immunoblotted for PTEN and ERK1/2, and densitometric quantitation of immunoblots is shown. *B*: Skeletal muscle and hepatic mRNA expression of pri-miR-21 and mature miR-21 from HFD-fed *Mkp-1*$^{fl/fl}$ and MKP1-MKO mice. Results represent n = 5 and 10/genotype for skeletal muscle and liver, respectively. *C*: C2C12 myoblasts were transfected with vector or constitutively active mutants of MKK6 (EE), MKK4 (EE), and MEK1. C2C12 myoblasts were analyzed for miR-21 expression or immunoblotted for phospho-(p)p38 MAPK, pJNK, and pERK1/2 with corresponding MAPK totals (n = 3). Data shown are the mean ± SEM. *$P < 0.05$; **$P <$ 0.01 as determined by Student t test. White bars, *Mkp-1*$^{fl/fl}$ mice; black bars, MKP1-MKO mice.

significantly increased in MKP1-MKO mice compared with *Mkp-1*$^{fl/fl}$ chow-fed mice (Fig. 8*C*). These results demonstrate that skeletal muscle MKP-1 plays a key role in negatively regulating the expression of genes involved in mitochondrial biogenesis.

To establish whether the enhanced expression of mitochondrial genes in skeletal muscles of MKP1-MKO mice improves oxidative mitochondrial capacity, we measured mitochondrial respiration in permeabilized myofibers. The respiratory control ratio (state 3, ADP-stimulated maximal respiration; state 4, basal mitochondria respiration) was found to be increased in MKP1-MKO mice in both chow- and HFD-fed mice as compared with HFD- and chow-fed *Mkp-1*$^{fl/fl}$ controls (Fig. 8*E*). These results suggest that skeletal muscle mitochondria from MKP1-MKO mice show improved ability to couple oxygen consumption to ATP synthesis (Fig. 8*E*). Although the expression of UCP3 in chow-fed MKP1-MKO and *Mkp-1*$^{fl/fl}$ control mice was comparable, a trend toward increased UCP3 expression was observed in HFD-fed MKP1-MKO mice as compared with *Mkp-1*$^{fl/fl}$ controls (Supplementary Fig. 6). Furthermore, mtDNA content is increased in skeletal muscle of both chow- and HFD-fed MKP1-MKO mice (Fig. 8*F*).

Finally, we examined endurance capacity in MKP1-MKO mice. The maximal amount of oxygen used at exhaustion (VO_{2max}) was significantly higher in MKP1-MKO mice (Fig. 8*G*). We also observed an increased running distance in the MKP1-MKO chow-fed mice as compared with *Mkp-1*$^{fl/fl}$ controls (Fig. 8*H*), and this correlated with reduced total body fat mass (Fig. 8*I*). Thus, MKP1-MKO mice have increased endurance capacity consistent with the notion that skeletal muscle MKP-1 acts to negatively regulate mitochondrial oxidative capacity and myofiber composition.

DISCUSSION

In this study, we show that MKP-1 is increased in its levels of expression in skeletal muscle of obese humans. MKP-1 is induced in many cases, if not all, by the same stressors that activate p38 MAPK and JNK to function in a negative-feedback pathway (18). Consistent with this, mice fed an HFD exhibit increased skeletal muscle MKP-1 expression and concomitant downregulation of p38 MAPK (22).

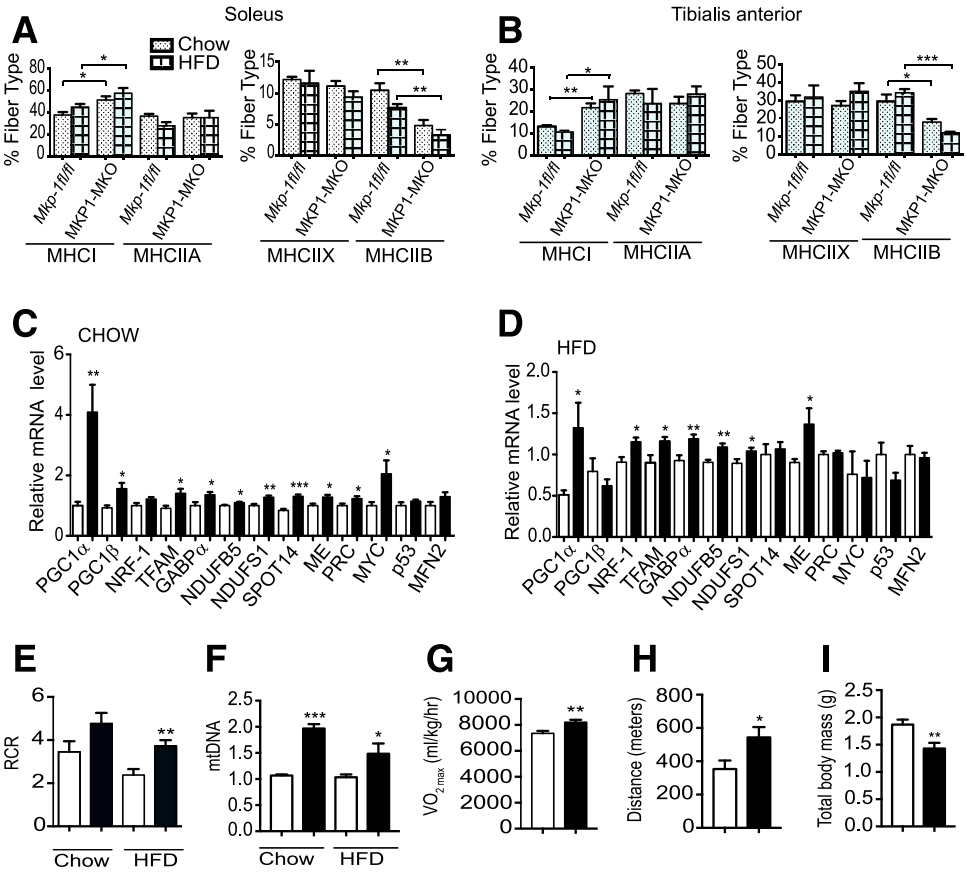

Figure 8—Enhanced skeletal muscle oxidative capacity, mitochondrial gene expression, and endurance in MKP1-MKO mice. Percentage of fiber type from soleus (*A*) and tibialis anterior (*B*) in chow- and HFD-fed *Mkp-1*$^{fl/fl}$ and MKP1-MKO mice (n = 6/genotype). mRNA expression of mitochondrial genes from chow-fed (*C*) and HFD-fed (*D*) *Mkp-1*$^{fl/fl}$ and MKP1-MKO mice (n = 6/genotype). *E*: Mitochondrial respiratory control ration (RCR) in chow- and HFD-fed *Mkp-1*$^{fl/fl}$ and MKP1-MKO mice (n = 6/genotype). *F*: mtDNA in chow- and HFD-fed *Mkp-1*$^{fl/fl}$ and MKP1-MKO mice (n = 5/genotype). Parameters during endurance exercise show in VO_{2max} (*G*), distance run during endurance exercise (*H*), and total body fat mass after exercise (*I*) in chow-fed *Mkp-1*$^{fl/fl}$ and MKP1-MKO mice (n = 7/genotype). Data represent mean ± SEM. *$P < 0.05$; **$P < 0.01$; ***$P < 0.0001$ as determined by as determined by Student t test. White bars, *Mkp-1*$^{fl/fl}$ mice; black bars, MKP1-MKO mice.

Interestingly, p38 MAPK has also been reported to be downregulated in the livers of HFD-fed mice, which is in line with the observation that hepatic MKP-1 is upregulated (23,32). Additionally, in obese human subjects, MKP-1 has been shown to be overexpressed in adipose tissue and macrophages with concomitant downregulation of p38 MAPK and PGC-1α (33). It is well established that the expression levels of adiponectin are negatively correlated with obesity (34). In skeletal muscle, adiponectin negatively regulates the expression of MKP-1 (35). Consistent with this, HFD-fed mice that have low levels of adiponectin exhibit reduced p38 MAPK-mediated activation of PGC-1α and reduced skeletal muscle mitochondrial biogenesis (35). Collectively, these observations are consistent with our findings and support a mechanism by which in obesity increased free fatty acids (22) and hypoadiponectin states promote reduced skeletal muscle oxidative metabolism by upregulating MKP-1.

By examining the composition of skeletal muscle myofibers, we found that there was an increase in the proportion of slow oxidative myofibers and a reduction in the proportion of fast glycolytic myofibers in skeletal muscle derived from MKP1-MKO mice. Thus, our results imply that changes in myofiber type composition could contribute to the enhanced oxidative and reduced glycolytic capacity of skeletal muscles of MKP1-MKO mice. Mitochondrial oxidation, ATP synthesis, and myofiber type composition contribute to the control of muscle endurance (36,37). MKP1-MKO mice were observed to exhibit significantly increased levels of endurance, which further supports the interpretation that the oxidative characteristics of these skeletal muscles is improved. Together, these observations provide an explanation for the increased levels of mitochondrial function and increased whole-body energy expenditure in MKP1-MKO mice and thus resistance to diet-induced obesity. It has been suggested that slow oxidative myofibers, which confer enhanced mitochondrial capacity, are more insulin sensitive than fast glycolytic myofibers (8,38). Moreover, studies have shown that decreased PGC-1α and NRF-1 levels correlate with insulin resistance and type 2 diabetes (39). Several studies have linked decreased mitochondrial biogenesis to

the pathogenesis of insulin resistance and type 2 diabetes (9,40). Consistent with this, MKP1-MKO mice are insulin sensitive when fed an HFD, which is consistent with that the increased percentage of slow oxidative myofibers and increased Akt in MKP1-MKO mice. In contrast, under chow-fed conditions, in which p38 MAPK and JNK activity were also increased in skeletal muscles of MKP1-MKO mice, we were unable to detect changes in the expression levels of the PTEN/Akt/miR-21 axis and subsequently differences in insulin-stimulated glucose homeostasis. These results indicate that loss of MKP-1 only under HFD conditions is sufficient to induce changes in the expression of the PTEN/Akt/miR-21 pathway. This could be due to the magnitude of p38 MAPK/JNK hyperactivation in the absence of MKP-1 in skeletal muscles of mice fed a chow diet as compared with those fed an HFD. Indeed, we observed that the increased levels of p38 MAPK/JNK activity are greater in MKP1-MKO mice fed an HFD as compared with those mice fed a chow diet. Loss of MKP-1 in skeletal muscle either in chow- or HFD-fed MKP1-MKO mice was sufficient to induce the expression of oxidative myofibers, suggesting that oxidative myofiber regulation may be engaged at a lower threshold of p38 MAPK/JNK hyperactivation than that required to influence the PTEN/Akt/miR-21 axis.

Because MKP-1 is nuclear localized, its ability to affect JNK-mediated phosphorylation of the insulin substrate receptor-1, and subsequently Akt-mediated glucose uptake, was not likely operable (20). However, MKP1-MKO mice have increased levels of Akt, which led us to uncover a pathway by which skeletal muscle MKP-1 negatively regulates Akt through miR-21 antagonism of PTEN (26). Both p38 MAPK and JNK activities are capable of stimulating not only miR-21 expression but also we found that the precursor, pri-miR-21, was also increased in expression. In addition to transcriptional activation, processing of pri-miRNAs occurs in the nucleus (27), suggesting that a nuclear-localized p38 MAPK/JNK mechanism exists in the regulation of either miRNA transcription and/or processing. Our data are consistent with a role of MKP-1 in miR-21 transcriptional regulation. Whether MKP-1 affects miR-21 processing cannot be ruled out because p38 MAPK has been implicated in the regulation of miRNA processing (41). Given that MKP-1 is overexpressed in skeletal muscle in obesity, these data suggest that insulin resistance could be promoted, at least in part, by MKP-1–mediated suppression of Akt through an MAPK/miR-21/PTEN pathway. It is also conceivable that a similar pathway of MKP-1 overexpression in macrophages in obese humans (33) may also exist, and this, too, contributes to insulin resistance. Interestingly, our studies demonstrate that skeletal muscle MKP-1 impacts hepatic function. We found that the livers of MKP1-MKO mice were protected from the accumulation of triglycerides and development of hepatic steatosis. Skeletal muscle is one of the major tissues responsible for hydrolysis of triglycerides; it is conceivable that protection from hepatic steatosis in the MKP1-MKO mice could be due to enhanced triglyceride hydrolysis in skeletal muscle, leading to reduced triglycerides in the blood and hence the phenotype in the liver.

Taken together, we demonstrate that skeletal muscle MKP-1 serves as a critical signaling node for both p38 MAPK and JNK. In obese states in which skeletal muscle MKP-1 is overexpressed, the data suggest that the integrated output of the p38 MAPK/JNK module is disrupted. Thus, reduced rather than increased p38 MAPK/JNK module signaling in skeletal muscle promotes insulin resistance and metabolic dysfunction.

Acknowledgments. The authors thank members of the Bennett laboratory for helpful discussions during the course of this study.

Funding. This work was supported by National Institute of Diabetes and Digestive and Kidney Diseases grant P01-DK-57751 (to A.M.B.), Yale University's Mouse Metabolic Phenotyping Center (grant U24-DK-59635), and the Yale Liver Center (grant P30-DK-34989).

Duality of Interest. No potential conflicts of interest relevant to this article were reported.

Author Contributions. A.L., K.M., L.Z., A.C.-D., M.J.J., J.P.G.C., and Y.N. performed experiments and analyzed data. A.L. and A.M.B. designed the experiments, reviewed all of the data, and wrote the manuscript. T.P.G., G.I.S., and C.H.-F. reviewed and edited the manuscript. A.M.B. is the guarantor of this work and, as such, had full access to all the data in the study and takes responsibility for the integrity of the data and the accuracy of the data analysis.

References

1. Bassel-Duby R, Olson EN. Signaling pathways in skeletal muscle remodeling. Annu Rev Biochem 2006;75:19–37

2. Zierath JR, Hawley JA. Skeletal muscle fiber type: influence on contractile and metabolic properties. PLoS Biol 2004;2:e348

3. Semenkovich CF. Insulin resistance and atherosclerosis. J Clin Invest 2006; 116:1813–1822

4. Samuel VT, Shulman GI. Mechanisms for insulin resistance: common threads and missing links. Cell 2012;148:852–871

5. Schiaffino S, Reggiani C. Fiber types in mammalian skeletal muscles. Physiol Rev 2011;91:1447–1531

6. Oberbach A, Bossenz Y, Lehmann S, et al. Altered fiber distribution and fiber-specific glycolytic and oxidative enzyme activity in skeletal muscle of patients with type 2 diabetes. Diabetes Care 2006;29:895–900

7. Pedersen BK, Febbraio MA. Muscles, exercise and obesity: skeletal muscle as a secretory organ. Nat Rev Endocrinol 2012;8:457–465

8. Stuart CA, McCurry MP, Marino A, et al. Slow-twitch fiber proportion in skeletal muscle correlates with insulin responsiveness. J Clin Endocrinol Metab 2013;98:2027–2036

9. Petersen KF, Dufour S, Befroy D, Garcia R, Shulman GI. Impaired mitochondrial activity in the insulin-resistant offspring of patients with type 2 diabetes. N Engl J Med 2004;350:664–671

10. Sabio G, Davis RJ. cJun NH2-terminal kinase 1 (JNK1): roles in metabolic regulation of insulin resistance. Trends Biochem Sci 2010;35:490–496

11. Manieri E, Sabio G. Stress kinases in the modulation of metabolism and energy balance. J Mol Endocrinol 2015;55:R11–R22

12. Solinas G, Becattini B. JNK at the crossroad of obesity, insulin resistance, and cell stress response. Mol Metab 2016;6:174–184

13. Pal M, Febbraio MA, Lancaster GI. The roles of c-Jun NH2-terminal kinases (JNKs) in obesity and insulin resistance. J Physiol 2016;594:267–279

14. Sabio G, Kennedy NJ, Cavanagh-Kyros J, et al. Role of muscle c-Jun NH2-terminal kinase 1 in obesity-induced insulin resistance. Mol Cell Biol 2010;30: 106–115

15. Xi X, Han J, Zhang JZ. Stimulation of glucose transport by AMP-activated protein kinase via activation of p38 mitogen-activated protein kinase. J Biol Chem 2001;276:41029–41034

16. Akimoto T, Pohnert SC, Li P, et al. Exercise stimulates Pgc-1alpha transcription in skeletal muscle through activation of the p38 MAPK pathway. J Biol Chem 2005;280:19587–19593
17. 1Nandipati KC, Subramanian S, Agrawal DK. Protein kinases: 1mechanisms and downstream targets in inflammation-mediated obesity and insulin resistance. Mol Cell Biochem 2017;426:27–45
18. Caunt CJ, Keyse SM. Dual-specificity MAP kinase phosphatases (MKPs): shaping the outcome of MAP kinase signalling. FEBS J 2013;280: 489–504
19. Lawan A, Bennett AM. MAP kinase phosphatases emerge as new players in metabolic regulation. In *Protein Tyrosine Phosphatase Control of Metabolism*. Bence KK, Ed. New York, Springer, 2013, p. 221
20. Wu JJ, Roth RJ, Anderson EJ, et al. Mice lacking MAP kinase phosphatase-1 have enhanced MAP kinase activity and resistance to diet-induced obesity. Cell Metab 2006;4:61–73
21. Flach RJ, Qin H, Zhang L, Bennett AM. Loss of mitogen-activated protein kinase phosphatase-1 protects from hepatic steatosis by repression of cell death-inducing DNA fragmentation factor A (DFFA)-like effector C (CIDEC)/fat-specific protein 27. J Biol Chem 2011;286:22195–22202
22. Roth RJ, Le AM, Zhang L, et al. MAPK phosphatase-1 facilitates the loss of oxidative myofibers associated with obesity in mice. J Clin Invest 2009;119: 3817–3829
23. Lawan A, Zhang L, Gatzke F, et al. Hepatic mitogen-activated protein kinase phosphatase 1 selectively regulates glucose metabolism and energy homeostasis. Mol Cell Biol 2015;35:26–40
24. Schwander M, Leu M, Stumm M, et al. Beta1 integrins regulate myoblast fusion and sarcomere assembly. Dev Cell 2003;4:673–685
25. Perdiguero E, Sousa-Victor P, Ruiz-Bonilla V, et al. p38/MKP-1-regulated AKT coordinates macrophage transitions and resolution of inflammation during tissue repair. J Cell Biol 2011;195:307–322
26. Meng F, Henson R, Wehbe-Janek H, Ghoshal K, Jacob ST, Patel T. MicroRNA-21 regulates expression of the PTEN tumor suppressor gene in human hepatocellular cancer. Gastroenterology 2007;133:647–658
27. Denli AM, Tops BB, Plasterk RH, Ketting RF, Hannon GJ. Processing of primary microRNAs by the Microprocessor complex. Nature 2004;432:231–235
28. Wu Z, Puigserver P, Andersson U, et al. Mechanisms controlling mitochondrial biogenesis and respiration through the thermogenic coactivator PGC-1. Cell 1999; 98:115–124
29. McAninch EA, Bianco AC. Thyroid hormone signaling in energy homeostasis and energy metabolism. Ann N Y Acad Sci 2014;1311:77–87
30. Morrish F, Hockenbery D. MYC and mitochondrial biogenesis. Cold Spring Harb Perspect Med 2014;4:a014225
31. Kim J, Lee JH, Iyer VR. Global identification of Myc target genes reveals its direct role in mitochondrial biogenesis and its E-box usage in vivo. PLoS One 2008;3:e1798
32. Lee J, Sun C, Zhou Y, et al. p38 MAPK-mediated regulation of Xbp1s is crucial for glucose homeostasis. Nat Med 2011;17:1251–1260
33. Khadir A, Tiss A, Abubaker J, et al. MAP kinase phosphatase DUSP1 is overexpressed in obese humans and modulated by physical exercise. Am J Physiol Endocrinol Metab 2015;308:E71–E83
34. Kadowaki T, Yamauchi T. Adiponectin and adiponectin receptors. Endocr Rev 2005;26:439–451
35. Qiao L, Kinney B, Yoo HS, Lee B, Schaack J, Shao J. Adiponectin increases skeletal muscle mitochondrial biogenesis by suppressing mitogen-activated protein kinase phosphatase-1. Diabetes 2012;61:1463–1470
36. Villena JA. New insights into PGC-1 coactivators: redefining their role in the regulation of mitochondrial function and beyond. FEBS J 2015;282:647–672
37. Puigserver P, Spiegelman BM. Peroxisome proliferator-activated receptor-gamma coactivator 1 alpha (PGC-1 alpha): transcriptional coactivator and metabolic regulator. Endocr Rev 2003;24:78–90
38. Crescenzo R, Bianco F, Mazzoli A, Giacco A, Liverini G, Iossa S. Mitochondrial efficiency and insulin resistance. Front Physiol 2015;5:512
39. Patti ME, Butte AJ, Crunkhorn S, et al. Coordinated reduction of genes of oxidative metabolism in humans with insulin resistance and diabetes: potential role of PGC1 and NRF1. Proc Natl Acad Sci U S A 2003;100:8466–8471
40. Morino K, Petersen KF, Dufour S, et al. Reduced mitochondrial density and increased IRS-1 serine phosphorylation in muscle of insulin-resistant offspring of type 2 diabetic parents. J Clin Invest 2005;115:3587–3593
41. Hong S, Noh H, Chen H, et al. Signaling by p38 MAPK stimulates nuclear localization of the microprocessor component p68 for processing of selected primary microRNAs. Sci Signal 2013;6:ra16